Supporting Information: Axisymmetric diffusion kurtosis imaging with Rician bias correction: A simulation study

Jan Malte Oeschger[1,*] Karsten Tabelow[2] Siawoosh Mohammadi[1,3]

September 1, 2022

1 University Medical Center Hamburg Eppendorf, Institute of Systems Neuroscience, Hamburg, Germany

2 Weierstrass Institute for Applied Analysis and Stochastics, Berlin, Germany

3 Max Planck Institute for Human Cognitive and Brain Sciences, Department of Neurophysics, Leipzig, Germany

***** Corresponding author:

Name	Jan Malte Oeschger
Institute	University Medical Center Hamburg-Eppendorf, Institute of Systems Neuroscience
Address	Martinistraße 52, 20246 Hamburg, Germany
E-mail	j.oeschger@uke.de
Phone	+49-40-7410-27301

S1 Supporting Information

S1.1 Parameter estimation and the Rician noise bias (detailed)

Standard DKI or axisymmetric DKI parameter estimation would typically be done using the acquired magnitude signals $S_{b,\vec{g}}$ and Eq. (2.1a, main text) or (2.3, main text) in the least-squares approach[1;2;3] (found fit results are denoted with a hat, i.e., $\hat{S}_0, \hat{D}, \hat{W}$):

$$(\hat{S}_0, \hat{D}, \hat{W}) = \text{argmin}_{\widetilde{S}_0, D, W} \sum_i (S_{b,\vec{g}_i} - \widetilde{S}_{b,\vec{g}_i}(\widetilde{S}_0, D, W))^2 \tag{S1.1}$$

However, this least-squares approach is built on the assumption of Gaussian distributed noise in $S_{b,\vec{g}_i}$ which is not true in reality. $S_{b,\vec{g}}$ is a magnitude signal computed from the noise contaminated k-space data described by a complex Gaussian (standard deviation σ) as the sum of squares of the measured signal intensity[4] from the receiver coil after it was Fourier transformed into real space. Computing the sum of squares rectifies the composite magnitude signal and leads to Rician distributed noise for one receiver coil (L= 1). Therefore, assuming Gaussian noise in MRI magnitude signals leads to a bias that propagates into the estimated parameters which is referred to as the "Rician noise bias". Eq. (S1.1) is therefore biased.

More generally, if one assumes uncorrelated noise and statistically independent receiver coils with an equivalent noise variance[5], the resulting probability density function of the noisy magnitude data is given by a non-central χ-distribution[4], where $2L$ is the number of degrees of freedom of the distribution. $L = 1$ results in the Rician distribution[6;7].

The severity of the Rician noise bias depends on the SNR[8] because the sum of squares rectifies the composite magnitude signal: the lower the SNR, the larger the bias. For RBC, we rely on an approach outlined in[8] that uses the expectation value $\mathbf{E}(S_{b,\vec{g}})$ of the noisy composite magnitude signal. The probability density function of $S_{b,\vec{g}}$ is a non-central χ distribution whose expectation value $\mathbf{E}(S_{b,\vec{g}})$ is given by[8]:

$$\mathbf{E}(S_{b,\vec{g}}) = \mathbf{E}(\widetilde{S}_{b,\vec{g}}(\widetilde{S}_0, D, W), \sigma) = \sigma\sqrt{\frac{\pi}{2}} \cdot \mathbf{L}_{1/2}^{(L-1)}(\frac{\widetilde{S}_{b,\vec{g}}(\widetilde{S}_0, D, W)^2}{2\sigma^2}) \qquad \text{[S1.2]}$$

where $\mathbf{L}_{1/2}^{(L-1)}(x) = \frac{\Gamma(L+1/2)}{\Gamma(3/2)\Gamma(L)}\mathbf{M}(-1/2, L, x)$ is the generalized Laguerre polynomial which can be expressed using a confluent hypergeometric function $\mathbf{M}$, the Gamma function Γ and the number of receiver coils L. Only for simplicity of notation, in the text we neglect any possible dependence of σ on b, $\vec{g}$ or location, the employed RBC algorithm used the same σ in every image voxel. The SNR dependent expectation value Eq. (S1.2) differs from the noise-free signal, $\mathbf{E}(\widetilde{S}_{b,\vec{g}}(\widetilde{S}_0, D, W), \sigma) > \widetilde{S}_{b,\vec{g}}(\widetilde{S}_0, D, W)$ with the difference decreasing with increasing SNR. Following[8], we implemented a time-efficient fitting algorithm that, unlike Equation (S1.1), accounts for Rician noise in magnitude dMRI data by solving the optimization problem:

$$(\hat{S}_0, \hat{D}, \hat{W}) = \text{argmin}_{\widetilde{S}_0, D, W} \sum_i (S_{b,\vec{g}_i} - \mathbf{E}(\widetilde{S}_{b,\vec{g}_i}(\widetilde{S}_0, D, W), \sigma))^2 \qquad \text{[S1.3]}$$

Estimating parameters this way is referred to as "quasi-likelihood" estimation and is denoted as "RBC ON" in this paper. It was shown, that parameter estimation using the non-central χ noise statistic in a quasi-likelihood framework yields asymptotically unbiased parameter estimates[9;8].

Rician bias corrected, standard DKI or axisymmetric DKI parameter estimation can be done by using Equation (2.1a, main text) or Equation (2.3, main text) to compute the noise-free signal predictions $\widetilde{S}_{b,\vec{g}}$, then using Equation (S1.2) to compute $\mathbf{E}(\widetilde{S}_{b,\vec{g}}(\widetilde{S}_0, D, W), \sigma)$ and finally minimize Equation (S1.3) to estimate the framework parameters $(\hat{S}_0, \hat{D}, \hat{W})$ for standard DKI or Ω for axisymmetric DKI.

In reality, noise correlations between receiver coils occur and are non-negligible, especially for a higher number of receiver coils (32 or 64). This affects the degrees of freedom of the underlying noise statistic. However, the non-central χ distribution can still be used as a good approximation, if an effective number of coils L_{eff} and noise variance σ^2_{eff} are used[5] for which $L \geq L_{\text{eff}}$ and $\sigma^2 \leq \sigma^2_{\text{eff}}$ can be shown. Similarly, the generalized autocalibrating partially parallel acquisition (GRAPPA) scheme can be accounted for by specifying an effective number of coils L_{eff}, while $L = 1$ for sensitivity encoding (SENSE)[5].

S1.2 Parameter estimation with the Gauss-Newton algorithm

To minimize Eq. (S1.1) or Eq. (S1.3) time-efficiently, we have implemented a Gauss-Newton minimization algorithm[10] in Matlab for slice-wise and parallelizable parameter estimation on MR-images instead of using standard Matlab optimization functions. The used tools are freely available online within the ACID toolbox (`http://www.diffusiontools.com/`) for SPM. Slice-wise fitting refers to fitting all voxels of an image-slice at the same time which improves run-time. The implemented algorithm is highly adaptable and can fit any signal model (especially non-linear models). Gauss Newton parameter estimation approximates the search direction in parameter space based on the Jacobian and is sensitive to the initial guess. For the initial guess of the axisymmetric DKI fit implementation, we used code from the repository of Sune Nørhøj Jespersen: `https://github.com/sunenj/Fast-diffusion-kurtosis-imaging-DKI`[11].

S1.3 Simulation study: Datasets and overview (detailed)

We assessed estimation accuracy of the five AxTM as a function of the SNR in a simulation study with two classes of datasets. The first class consisted of three synthetic voxels with varying fiber alignment (defined in[12]). This dataset is refereed to as "`synthetic dataset`" because it was derived in the context of another study[12] by random sampling of the parameter space of biophysical parameters and consequent derivation of the corresponding AxTM. The other class of datasets was based on an in-vivo measurement and consisted of either twelve major white matter fiber tract voxels ("`in-vivo white matter dataset`") or twelve voxels from typical gray matter areas ("`in-vivo gray matter dataset`"). Details on both classes of datasets are given below and in Figure 2 (main manuscript). For all datasets, magnitude diffusion MRI data were simulated for varying SNRs and fitted with standard DKI and axisymmetric DKI, with and without RBC (as described in Section 2.3, main manuscript or Section S1.1) to obtain estimates of the five AxTM. Accuracy of the obtained AxTM estimates were evaluated as the absolute value of the mean percentage error (A-MPE):

$$\text{A-MPE} = 100 \cdot \frac{\mid \text{GT} - \overline{\text{FitResults}}(\text{SNR}) \mid}{\text{GT}} \qquad \text{[S1.4]}$$

Here GT refers to the ground truth and $\overline{\text{FitResults}}$ refers to the average of the fit results over the noise samples. We evaluated the accuracy of the AxTM estimates for each estimation method by looking for the SNR after which the A-MPE was smaller 5%. The 5% threshold was considered an acceptable error in a trade-off between estimation accuracy and SNR requirement. The different setup of both simulation studies enables an isolated investigation of the effectiveness and tissue dependence of the RBC and to test the fitting methods in in-vivo data. As a summary to compare each method, we looked at the maximum SNR needed across the five AxTM for which A-MPE consistently $< 5\%$ for all AxTM ("Maximum" column in Figure 6, main manuscript).

Datasets: The `synthetic dataset` consisted of three synthetic sets of AxTM (from[12]) describing three voxels with varying fiber alignment, one with fibers with low alignment ("LA", FA=0.067), one with fibers with moderate alignment ("MA", FA=0.24) and one with highly aligned fibers ("HA", FA=0.86). The AxTM of the three synthetic voxels are summarized in Supporting Information Table S1. Figure 4 (main manuscript) shows two areas of typical brain regions in a map of the mean of the kurtosis tensor $\overline{W}$ where LA and HA voxels can be found and the corresponding idealized fiber stick model.

The simulated `in-vivo white matter dataset` is based on an in-vivo DWI measurement with the following measurement parameters: The sequence was a mono-polar single-shot spin-echo EPI scheme, consisting of 16 non-diffusion-weighted images ($b = 0$ image). The diffusion weighted images were acquired at three b values (500s/mm^2, 1250s/mm^2, 2500s/mm^2), sampled for 60 unique diffusion-gradient directions for the 1250s/mm^2 and 2500s/mm^2 shells and 30 unique directions for the 500s/mm^2 shell. The entire protocol was repeated with reversed phase encoding directions ("blip-up", "blip-down" correction) to correct for susceptibility-related distortions so that in total $166 \cdot 2$ images were acquired. Other acquisition parameters were: an isotropic voxel size of (1.6mm^3), FoV of 240x230x154mm^3, TE = 73ms, TE = 5300ms and 7/8 partial Fourier imaging. Signal simulation in our simulation study was done with only one $b = 0$ signal, so that the simulated sequence consisted of 151 signals per noise realization.

The `in-vivo white matter dataset` consists of twelve voxels extracted from four major white matter tracts (three voxels from each of the four fiber tracts, see Figure 3, main manuscript) from an in-vivo brain measurement (SNR=23.4) of a healthy volunteer. The twelve voxels were extracted from the in-vivo measurement by fitting the standard DKI framework in 12 white matter voxels of the acquired in-vivo DWI magnitude images to get the corresponding 22 standard DKI tensor metrics, the derived data are therefore referred to as "in-vivo white matter". Three voxels each with HA to MA (defined through the fractional anisotropy (FA) threshold FA≥ 0.4[13]) were extracted from these four major white matter fiber tracts based upon the Jülich fiber atlas: the callosum body (`cb`), the corticospinal tract (`ct`), the optic radiation (`or`) and the superior longitudinal fasciculus (`slf`), see Figure 3, main manuscript. The selected voxels differ from the synthetic voxels in that here only HA and MA voxels were selected. The sets of the 12x22 in-vivo white matter standard DKI tensor metrics are documented in Table S2, the derived AxTM are found in Table S3.

The `in-vivo gray matter dataset` was produced according to the same procedure used for the `in-vivo white matter dataset`, only that the voxels were selected from typical gray matter areas. The sets of the 12x22 in-vivo gray matter standard DKI tensor metrics are documented in Supporting Information Table S4, the derived AxTM are found in Supporting Information Table S5. Since white matter is the focus of this manuscript, details and results on the `in-vivo gray matter dataset` can be found in Supporting Information Section S1.3.

Signal framework used for simulation: The three synthetic voxels of AxTM were simulated with the axisymmetric DKI framework to first obtain noise-free diffusion MRI signals $\widetilde{S}_{\text{noise-free}}$. The twelve in-vivo white matter and gray matter voxels were simulated with the standard DKI framework to first obtain noise-free diffusion MRI signals $\widetilde{S}_{\text{noise-free}}$.

Contamination with noise: For both the `synthetic` and the `in-vivo dataset` (white matter or gray matter), the noise-free diffusion MRI signals $\widetilde{S}_{\text{noise-free}}$ were contaminated with noise for SNRs $[1, 2, 3...200]$ and magnitude signals S_{cont} were computed. The noisy magnitude signals were computed according to $S_{\text{cont}} = |\widetilde{S}_{\text{noise-free}} + \alpha + \beta i|$, where $\alpha, \beta \in \mathcal{N}(0, \sigma)$ are drawn from a zero mean Gaussian with standard deviation σ, yielding different $\text{SNR} = \sqrt{2}S_0/\sigma$ (for one receiver coil) for a given $S_0 = 1$.

Estimating the five AxTM: Both, the simulated signals S_{cont} from the `synthetic` and the `in-vivo dataset` were fitted with axisymmetric DKI and standard DKI, with and without RBC (Section 2.3, main manuscript or Section S1.1) to obtain estimates of the AxTM whose accuracy could then be investigated as a function of SNR.

S1.4 Simulation studies: Details

We simulated 200 SNRs: SNR = $[1, 2, 3, ...200]$. Noise was added according to $S_{\text{cont}} = |\widetilde{S}_{\text{noise-free}} + \alpha + \beta i|$, where $\alpha, \beta \in \mathcal{N}(0, \sigma)$ are drawn from a zero mean Gaussian with standard deviation σ, yielding different $\text{SNR} = \sqrt{2}\frac{S_0}{\sigma}$ (for one receiver coil) for a given $S_0 = 1$. For every SNR, 2500 noise samples were realized, i.e., $2500 \cdot 151$ pairs (α, β) were drawn and $2500 \cdot 151$ S_{cont} were calculated per SNR for every simulated voxel. These diffusion MRI magnitude signals were then fitted with the four proposed methods. For each of the 2500 noise samples per SNR, 2500 parameter estimates of $D_{\|}, D_{\perp}, W_{\|}, W_{\perp}, \overline{W}$ were obtained and averaged to find the SNR above which the average over these 2500 noise samples had a A-MPE $< 5\%$ (`synthetic datset`). For the `in-vivo datsets` the A-MPE was averaged per SNR across the 12 simulated voxels and the SNR above which this averaged A-MPE $< 5\%$ is reported.

For simulation of the three synthetic voxels, the axis of symmetry $\vec{c} = (1, 0, 0)^T$ was fixed throughout the study. For data fitting, the two angles θ and ϕ that define the axis of symmetry within the axisymmetric DKI framework were variable but constrained to $\theta, \phi \in [-2\pi, 2\pi]$ which improved convergence of the fitting algorithm. Data were simulated according to the simulation scheme described in (Section 2.5, main text).

S1.5 Simulation of in-vivo gray matter

To test whether the results found for the "LA" voxel translates to in-vivo applications, we additionally performed a simulation and analysis of in-vivo gray matter voxels according to the same procedure already used for the in-vivo white matter simulation. For this, 12 voxels were extracted from four gray matter areas (three voxels from each gray matter area) analogously to extraction of the white matter voxels described in Section 2.5 in the main text. The four gray matter areas were the frontal cortex (fc), the motor cortex (mc), the thalamus (th) and the visual cortex (vc).

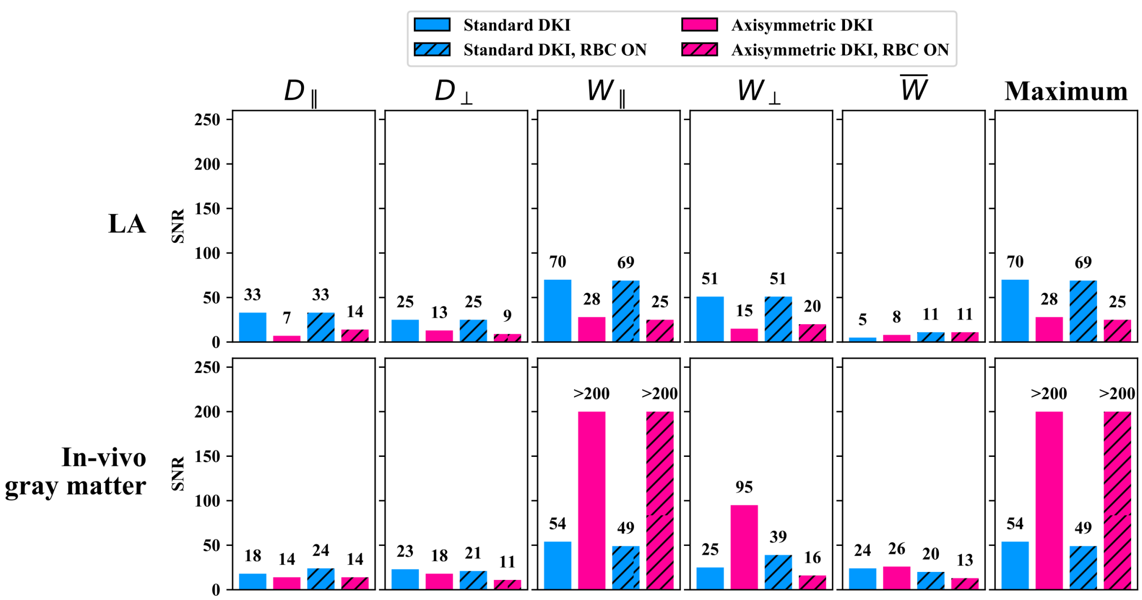

Figure S1: Signal-to-noise ratio (SNR) above which the absolute value of the mean percentage error (A-MPE, Eq. (2.8) in main text) $<$ 5% for the `in-vivo gray matter dataset` (bottom) and for the LA synthetic voxel (top). For the `in-vivo gray matter dataset` the A-MPE was computed in accordance with the procedure for the `in-vivo white matter dataset`, i.e., the A-MPE was averaged across the 12 simulated in-vivo gray matter voxels and the SNR above which this average A-MPE $<$ 5% is shown. The number above the barplots indicates the barplot's height. Blue encodes standard DKI, red encodes axisymmetric DKI, the hatched barplots show the results if RBC is used. "Maximum" shows the maximum SNR needed to achieve A-MPE $<$ 5% across all five AxTM.

Results:

Axisymmetric DKI not clearly superior to standard DKI in in-vivo gray matter: Estimation of $D_{||}$ and $D_{\perp}$ was improved by using the axisymmetric DKI framework instead of standard DKI. E.g., it only required an SNR$=14$ (axisymmetric DKI) instead of SNR$=18$ (standard DKI) to achieve A-MPE $<5\%$ for $D_{||}$. However, axisymmetric DKI performed much worse than standard DKI for $W_{||}$ where it needed SNRs above 200 to achieve A-MAPE $<5\%$ both with and without RBC which is in contrast to the results found for the synthetic "LA" dataset (see Figure S1). Another difference to the synthetic "LA" dataset is that RBC could substantially improve performance of the axisymmetric DKI framework for $W_{\perp}$ where it reduced the SNR requirements from 95 without RBC to 16 with RBC.

S1.6 Evaluation of precision

Analogous the absolute value of the mean percentage error (A-MPE) for the bias, we have quantified the precision of the four investigated methods (standard DKI and axisymmetric DKI with and without RBC) by calculating the standard deviation in reference to the ground truth (R-STD): $\text{R-STD} = 100 \cdot \frac{\text{std}(\text{Distribution}_{\text{Estimator}})}{\text{GroundTruth}}$. Here $\text{std}(\text{Distribution}_{\text{Estimator}})$ is the standard deviation over the distribution of fit results for each AxTM per method and SNR. The distribution of fit results for a specific AxTM per method and SNR is made up of the 2500 fit results obtained from the simulated 2500 noise samples per SNR. Analogous to the evaluation of the A-MPE, we were then interested to see at what SNR the R-STD$< 5\%$, i.e., at what SNR is the precision of a certain method within 5% of the corresponding ground truth value. We did this analysis for the in-vivo white matter and synthetic voxels (Figure S2). We additionally calculated the outlier-robust version of the R-STD, the "R-IQR", $\text{R-IQR} = 100 \cdot \frac{\frac{\text{IQR}(\text{Distribution}_{\text{Estimator}})}{1.3490}}{\text{GroundTruth}}$. Here $\text{IQR}(\text{Distribution}_{\text{Estimator}})$ is the interquartile range[14] of the distribution of fit results and the computed quantity $\frac{\text{IQR}(\text{Distribution}_{\text{Estimator}})}{1.3490}$ is a robust estimator for the standard deviation and hence the precision.

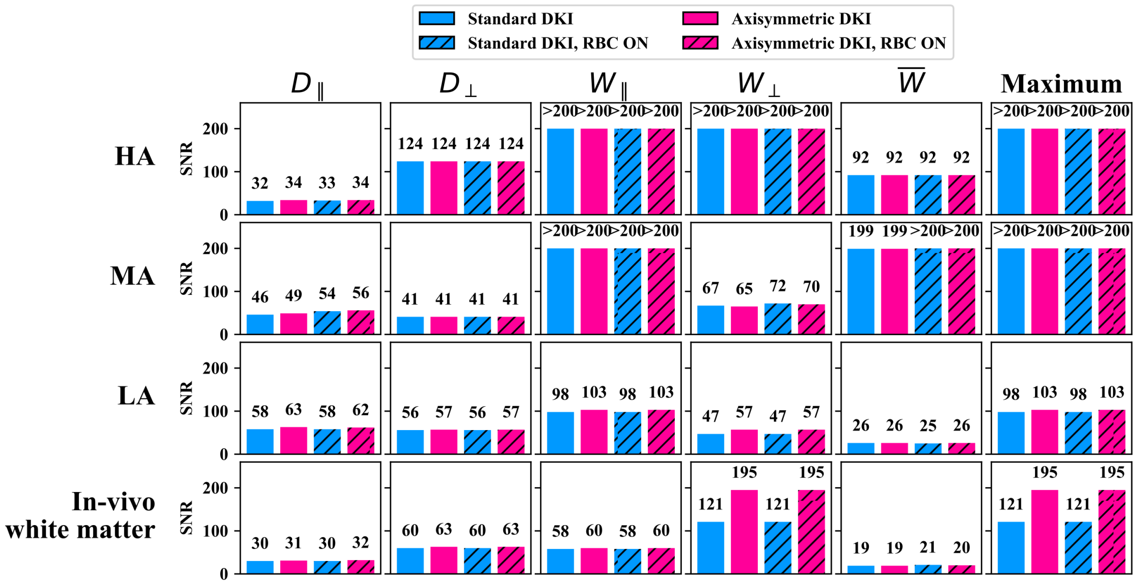

Figure S2: Signal-to-noise ratio (SNR) above which the standard deviation in reference to the ground truth (R-STD) $<5\%$ for the `synthetic dataset` with high, medium and low fiber alignment ("HA", "MA", "LA") and the `in-vivo white matter dataset`. For the `in-vivo white matter dataset`, the R-STD was averaged across the 12 simulated voxels and the SNR above which this average R-STD $<5\%$ is shown. The number above the barplots indicates the barplot's height. Blue encodes standard DKI, red encodes axisymmetric DKI, the hatched barplots show the results if RBC is used. "Maximum" shows the maximum SNR needed to achieve R-STD $<5\%$ across all five AxTM.

Results:

Precision is not improved by RBC or axisymmetric DKI: Generally, higher SNRs were required to reach the R-STD$<5\%$ threshold than reaching the A-MPE $<5\%$ threshold. Within each dataset (HA, MA, LA, in-vivo white matter) and for each AxTM, all four methods almost always performed very similar to each other, regardless of RBC or DKI framework. A larger difference between methods was only observed for $W_\perp$ of the `in-vivo white matter dataset` where standard DKI both with and without RBC required an SNR of 121 to reach the R-STD$<5\%$ threshold while axisymmetric DKI both with and without RBC required an SNR of 195, see Figure S2. Further investigation of this case revealed that the axisymmetric DKI fit results were affected by outliers for $W_\perp$ in the `in-vivo white matter dataset`. Figure S3 shows the outlier-robust R-IQR computed for the synthetic and the `in-vivo white matter dataset`. It can be seen that in this case the in-vivo white matter results for $W_{\perp}$ obtained with both DKI frameworks are similar (SNR of 120 for standard DKI and 119 for axisymmetric DKI). Since estimation of the R-IQR is an outlier-robust measure for the R-STD, this finding indicates that the observed difference in SNR requirements between standard DKI and axisymmetric DKI for $W_{\perp}$ in Figure S2 was caused by outliers in the results of the axisymmetric DKI fit.

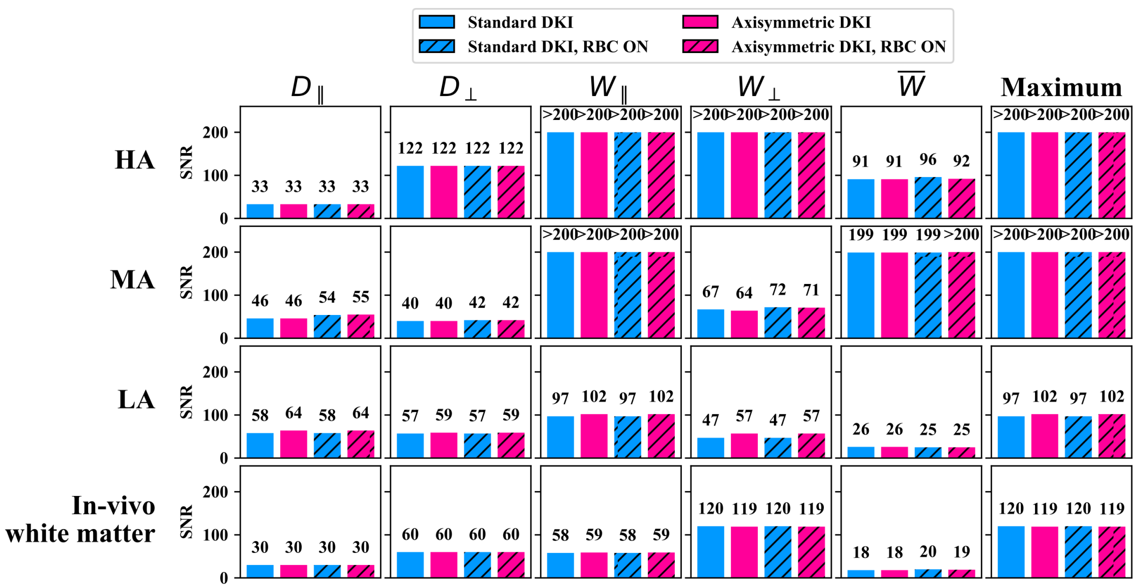

Figure S3: Signal-to-noise ratio (SNR) above which the R-IQR $< 5\%$ for the `synthetic dataset` with high, medium and low fiber alignment ("HA", "MA", "LA") and the `in-vivo white matter dataset`. For the `in-vivo white matter dataset`, the R-IQR was averaged across the 12 simulated voxels and the SNR above which this average R-IQR $< 5\%$ is shown. The number above the barplots indicates the barplot's height. Blue encodes standard DKI, red encodes axisymmetric DKI, the hatched barplots show the results if RBC is used. "Maximum" shows the maximum SNR needed to achieve R-IQR $< 5\%$ across all five AxTM.

S1.7 Ground truth DKI datasets

Table S1: Set of synthetic AxTM, $\widetilde{S}_0$ and axis of symmetry $\vec{c}$ used to simulate the `synthetic dataset` based on axisymmetric DKI. The `synthetic dataset` consisting of three voxels with sets of $\{D_{\|}, D_{\perp}, W_{\|}, W_{\perp}, \overline{W}\}$ was taken from[12], diffusivities are in $[\frac{\mathrm{\mu m}^2}{\mathrm{ms}}]$, S_0 is in arbitrary units.

Dataset	$D_{\|}$	$D_{\perp}$	$W_{\|}$	$W_{\perp}$	$\overline{W}$	$\widetilde{S}_0$	$\vec{c}$
Fibers with high alignment (HA)	1.503	0.195	1.456	0.291	0.926	1	$(1,0,0)^T$
Fibers with moderate alignment (MA)	1.557	1.048	0.396	0.708	0.330	1	$(1,0,0)^T$
Fibers with low alignment (LA)	0.457	0.408	2.901	2.702	2.770	1	$(1,0,0)^T$

Table S2: Ground truth in-vivo standard DKI voxels for the `in-vivo white matter dataset` (Figure 3, main text), shown are the diffusion and kurtosis tensor components and $\widetilde{S}_0$, the diffusivities are in $[\frac{\mathrm{\mu m}^2}{\mathrm{ms}}]$.

Parameter	cb voxel 1	cb voxel 2	cb voxel 3	ct voxel 1	ct voxel 2	ct voxel 3
D_{11}	1.92726	1.62057	1.86790	0.53951	0.78384	0.73087
D_{22}	0.31583	0.38127	0.41435	0.36193	0.42447	0.49957
D_{33}	0.39808	0.39813	0.36425	1.54966	1.37428	1.29096
D_{12}	−0.00731	−0.26198	−0.11110	−0.15777	−0.08699	−0.05191
D_{13}	0.04079	−0.25240	0.09536	0.00094	−0.08181	−0.03291
D_{23}	0.03170	−0.09149	−0.03971	−0.04121	0.15430	0.03331
$\widetilde{S}_0$	1.00000	1.00000	1.00000	1.00000	1.00000	1.00000
W_{1111}	4.26728	4.20207	3.73642	0.58735	1.16398	1.12725
W_{2222}	0.30183	0.43656	0.36961	0.22285	0.51330	0.74976
W_{3333}	0.43632	0.59204	0.26940	3.41702	2.14949	2.30314
W_{1112}	−0.15654	−0.41618	−0.18526	−0.07888	−0.06150	−0.08996
W_{1113}	0.10051	−0.64422	0.18910	0.00636	−0.02166	0.02767
W_{2221}	0.19206	−0.46340	−0.26578	−0.08910	−0.06061	−0.09517
W_{3331}	−0.08171	−0.15145	0.12274	−0.08214	−0.17008	−0.09078
W_{2223}	0.06537	−0.17548	−0.08403	0.09611	0.10937	−0.04710
W_{3332}	0.07430	−0.16995	−0.09129	−0.12567	0.28125	−0.09293
W_{1122}	0.45163	0.51896	0.50221	0.20913	0.21167	0.25976
W_{1133}	0.45000	0.53712	0.43661	0.52253	0.56751	0.30986
W_{2233}	0.15867	0.16724	0.07048	0.32234	0.42040	0.39227
W_{1123}	−0.00501	−0.08834	−0.03636	0.07669	0.03705	−0.00512
W_{2213}	−0.00262	0.00521	0.08195	−0.02098	−0.08206	−0.02479
W_{3312}	0.03732	−0.13410	−0.11029	−0.16710	−0.06077	−0.02733

Parameter	or voxel 1	or voxel 2	or voxel 3	slf voxel 1	slf voxel 2	slf voxel 3
D_{11}	1.06085	0.67273	0.69468	0.46699	0.68565	0.63911
D_{22}	0.59047	0.75000	1.79639	0.43803	0.48026	0.61127
D_{33}	1.36088	1.48673	0.49756	1.69614	1.23269	1.22297
D_{12}	0.12149	0.04143	−0.43159	0.05648	0.02784	0.08187
D_{13}	0.61736	0.22247	0.19896	0.07981	−0.07817	−0.04450
D_{23}	0.05184	0.26023	−0.21783	−0.20355	−0.15512	−0.09252
$\widetilde{S}_0$	1.00000	1.00000	1.00000	1.00000	1.00000	1.00000
W_{1111}	1.18421	0.74417	0.60364	0.38485	1.27168	0.65976
W_{2222}	0.48582	0.71486	2.21601	0.51498	0.72106	0.83091
W_{3333}	1.72750	1.99702	0.37346	3.25042	2.56281	1.96113
W_{1112}	0.09557	0.04945	−0.18369	0.03519	0.11477	0.00824
W_{1113}	0.42320	0.11965	0.04012	0.01711	0.05484	0.06571
W_{2221}	0.22072	−0.01878	−0.49678	0.11049	−0.03851	−0.10122
W_{3331}	0.70421	0.13580	0.03943	0.15730	−0.32397	−0.13608
W_{2223}	0.13593	−0.00500	−0.40378	−0.02510	0.06858	0.06213
W_{3332}	0.15332	0.36637	0.09475	−0.41687	−0.24668	−0.29428
W_{1122}	0.19154	0.25614	0.52836	0.12737	0.22065	0.18565
W_{1133}	0.61697	0.26980	0.15419	0.49145	0.36651	0.53366
W_{2233}	0.26455	0.40726	0.34763	0.42856	0.14162	0.27141
W_{1123}	0.04012	0.00642	−0.11345	−0.04016	−0.01867	−0.08256
W_{2213}	0.06872	0.07859	0.24902	−0.01085	−0.04099	0.02417
W_{3312}	0.02283	0.04014	−0.03715	0.06156	0.07493	0.17797

Table S3: Ground truth AxTM of the `in-vivo dataset`, corresponding to the tensor components listed in Table S2, the diffusivities are in $[\frac{\mu m^2}{ms}]$. Additionally, the deviation from axial symmetry is listed as $\frac{|\lambda_2-\lambda_3|}{MD}$, where λ are the diffusion tensor eigenvalues and MD is the mean diffusivity.

Voxel	$D_\parallel$	$D_\perp$	$W_\parallel$	$W_\perp$	$\overline{W}$	$\frac{|\lambda_2-\lambda_3|}{MD}$
cb voxel 1	1.928	0.356	4.276	0.401	1.425	0.117
cb voxel 2	1.714	0.343	4.549	0.387	1.535	0.346
cb voxel 3	1.883	0.382	3.798	0.240	1.279	0.091
ct voxel 1	1.551	0.450	3.427	0.471	1.267	0.444
ct voxel 2	1.413	0.585	2.373	0.762	1.245	0.461
ct voxel 3	1.295	0.613	2.294	0.903	1.221	0.299
or voxel 1	1.857	0.578	2.891	0.463	1.109	0.126
or voxel 2	1.623	0.643	2.244	0.706	1.064	0.074
or voxel 3	1.995	0.497	2.959	0.498	1.051	0.251
slf voxel 1	1.732	0.435	3.421	0.439	1.249	0.170
slf voxel 2	1.275	0.562	2.715	0.919	1.203	0.283
slf voxel 3	1.242	0.616	2.153	0.725	1.087	0.185

Table S4: Ground truth in-vivo standard DKI voxels for the `in-vivo gray matter dataset`, shown are the diffusion and kurtosis tensor components and $\widetilde{S}_0$, the diffusivities are in $[\frac{\mu m^2}{ms}]$.

Parameter	fc voxel 1	fc voxel 2	fc voxel 3	mc voxel 1	mc voxel 2	mc voxel 3
D_{11}	2.50277	1.31597	2.79424	1.61384	1.11080	1.47339
D_{22}	2.63215	1.42647	2.91701	1.54804	1.08889	1.53996
D_{33}	2.64935	1.40526	3.05176	1.51739	0.97417	1.40661
D_{12}	−0.03462	−0.00900	0.01455	0.01249	0.02530	0.02278
D_{13}	0.07854	0.04254	−0.02458	−0.06448	0.03418	−0.02653
D_{23}	−0.06748	0.01904	0.06747	−0.06417	0.02150	0.00347
$\widetilde{S}_0$	1.00000	1.00000	1.00000	1.00000	1.00000	1.00000
W_{1111}	0.56370	0.71667	0.42047	0.79404	0.89151	0.74619
W_{2222}	0.58092	0.93726	0.54043	0.65753	0.91672	0.86487
W_{3333}	0.62256	0.86199	0.53516	0.72181	0.84637	0.62263
W_{1112}	−0.00158	0.06715	−0.01741	−0.05272	0.05849	−0.02434
W_{1113}	0.02441	0.03391	0.00434	−0.02477	−0.03365	−0.02214
W_{2221}	−0.00470	−0.03735	0.02543	−0.02886	0.01141	0.03757
W_{3331}	0.01530	−0.01568	−0.01119	−0.01303	0.04189	0.04724
W_{2223}	−0.00684	0.02774	0.00758	−0.02444	0.03554	−0.02079
W_{3332}	−0.00801	−0.00802	0.01668	−0.00738	0.10307	0.05838
W_{1122}	0.19703	0.32119	0.15041	0.19543	0.33747	0.27489
W_{1133}	0.18887	0.32222	0.16831	0.21814	0.35201	0.23772
W_{2233}	0.19620	0.36126	0.15564	0.22378	0.34395	0.30244
W_{1123}	−0.00581	−0.02205	−0.00321	−0.02123	0.00832	−0.04963
W_{2213}	0.00504	0.02109	0.00011	−0.01980	0.04589	−0.01298
W_{3312}	0.00350	−0.02690	−0.00496	0.01040	0.02448	−0.00446

Parameter	th voxel 1	th voxel 2	th voxel 3	vc voxel 1	vc voxel 2	vc voxel 3
D_{11}	1.55114	0.85394	0.66375	1.11690	1.33449	1.58681
D_{22}	1.85125	0.83582	0.83513	1.12416	1.20188	1.61950
D_{33}	1.73899	0.99126	0.72202	1.19876	1.35827	1.53273
D_{12}	0.09370	−0.02131	0.04164	0.04721	−0.09738	−0.04635
D_{13}	0.07596	−0.07940	−0.03502	−0.03314	−0.05108	0.03868
D_{23}	−0.09738	−0.06603	0.03045	−0.05430	0.00351	0.02261
$\widetilde{S}_0$	1.00000	1.00000	1.00000	1.00000	1.00000	1.00000
W_{1111}	0.74150	1.02877	1.07671	0.90363	0.74407	0.63246
W_{2222}	0.88619	1.40701	1.34001	0.69061	0.57022	0.82642
W_{3333}	0.84407	1.28545	1.50206	0.80784	0.83729	0.60003
W_{1112}	0.02028	0.14173	0.27765	0.05292	−0.09488	−0.09342
W_{1113}	0.03574	−0.04782	−0.01630	−0.03856	−0.07960	−0.02566
W_{2221}	0.05168	−0.09366	0.09460	−0.08445	−0.07263	0.02135
W_{3331}	0.03040	−0.12668	−0.18875	0.00338	−0.01054	0.03591
W_{2223}	0.01033	−0.04656	0.19234	−0.02794	−0.00807	−0.00253
W_{3332}	−0.06420	−0.16355	0.09208	−0.00390	−0.02928	0.06912
W_{1122}	0.27604	0.37859	0.75919	0.27710	0.32099	0.20954
W_{1133}	0.26147	0.48093	0.47265	0.27969	0.29104	0.27671
W_{2233}	0.29981	0.31864	0.61072	0.25239	0.26290	0.24716
W_{1123}	−0.01479	0.02698	−0.04394	0.03306	−0.05787	−0.04289
W_{2213}	−0.00818	−0.05220	−0.18916	−0.00695	0.01136	−0.01380
W_{3312}	0.01688	−0.03173	0.06075	0.00558	−0.03849	0.00490

Table S5: Ground truth AxTM of the `gray matter in-vivo dataset`, corresponding to the tensor components listed in Table S2, the diffusivities are in $[\frac{\mu m^2}{ms}]$. Additionally, the deviation from axial symmetry is listed as $\frac{|\lambda_2 - \lambda_3|}{MD}$, where λ are the diffusion tensor eigenvalues and MD is the mean diffusivity.

Voxel	$D_\parallel$	$D_\perp$	$W_\parallel$	$W_\perp$	$\overline{W}$	$\frac{\lvert\lambda_2-\lambda_3\rvert}{MD}$
fc Dataset 1	2.738	2.523	0.623	0.560	0.586	0.042
fc Dataset 2	1.440	1.354	1.004	0.880	0.905	0.082
fc Dataset 3	3.081	2.841	0.543	0.466	0.489	0.036
mc Dataset 1	1.662	1.509	0.743	0.669	0.690	0.070
mc Dataset 2	1.137	1.018	1.066	0.878	0.944	0.102
mc Dataset 3	1.547	1.436	0.900	0.714	0.773	0.054
th Dataset 1	1.914	1.614	0.922	0.764	0.829	0.153
th Dataset 2	1.041	0.820	1.519	1.130	1.216	0.102
th Dataset 3	0.849	0.686	1.556	1.257	1.521	0.139
vc Dataset 1	1.248	1.096	0.796	0.799	0.804	0.043
vc Dataset 2	1.422	1.237	0.920	0.701	0.780	0.136
vc Dataset 3	1.652	1.543	0.751	0.638	0.705	0.058

References

[1] A. Tabesh, J. H. Jensen, B. A. Ardekani, and J. A. Helpern, "Estimation of tensors and tensor-derived measures in diffusional kurtosis imaging," *Magnetic Resonance in Medicine*, vol. 65, no. 3, pp. 823–836, 2011.

[2] J. Veraart, J. Sijbers, S. Sunaert, A. Leemans, and B. Jeurissen, "Weighted linear least squares estimation of diffusion MRI parameters: Strengths, limitations, and pitfalls," *NeuroImage*, vol. 81, pp. 335–346, Nov. 2013.

[3] S. Mohammadi, K. Tabelow, L. Ruthotto, T. Feiweier, J. Polzehl, and N. Weiskopf, "High-resolution diffusion kurtosis imaging at 3T enabled by advanced post-processing," *Frontiers in Neuroscience*, vol. 8, 2015.

[4] C. D. Constantinides, E. Atalar, and E. R. McVeigh, "Signal-to-noise measurements in magnitude images from NMR phased arrays," *Magnetic Resonance in Medicine*, vol. 38, pp. 852–857, 12 1997.

[5] S. Aja-Fernández and A. Tristán-Vega, "Influence of noise correlation in multiple-coil statistical models with sum of squares reconstruction," *Magnetic Resonance in Medicine*, vol. 67, no. 2, pp. 580–585, 2012.

[6] S. O. Rice, "Mathematical analysis of random noise," *Bell System Technical Journal*, vol. 23, no. 3, pp. 282–332, 1944.

[7] H. Gudbjartsson and S. Patz, "The Rician distribution of noisy MRI data," *Magnetic Resonance in Medicine*, vol. 34, no. 6, pp. 910–914, 1995.

[8] J. Polzehl and K. Tabelow, "Low SNR in Diffusion MRI Models," *Journal of the American Statistical Association*, vol. 111, no. 516, pp. 1480–1490, 2016.

[9] H. Bunke and W. Schmidt, "Asymptotic results on nonlinear approximation of regression functions and weighted least squares," *Series Statistics*, vol. 11, no. 1, pp. 3–22, 1980.

[10] J. Modersitzki, *FAIR: Flexible Algorithms for Image Registration*. Philadelphia: SIAM, 2009.

[11] B. Hansen, N. Shemesh, and S. N. Jespersen, "Fast imaging of mean, axial and radial diffusion kurtosis," *NeuroImage*, vol. 142, pp. 381–393, Nov. 2016.

[12] S. Coelho, J. M. Pozo, S. N. Jespersen, D. K. Jones, and A. F. Frangi, "Resolving degeneracy in diffusion MRI biophysical model parameter estimation using double diffusion encoding," *Magnetic Resonance in Medicine*, vol. 82, no. 1, pp. 395–410, 2019.

[13] A. Benitez, E. Fieremans, J. H. Jensen, M. F. Falangola, A. Tabesh, S. H. Ferris, and J. A. Helpern, "White matter tract integrity metrics reflect the vulnerability of late-myelinating tracts in Alzheimer's disease," *NeuroImage : Clinical*, vol. 4, pp. 64–71, Nov. 2013.

[14] P. J. Rousseeuw and C. Croux, "Alternatives to the Median Absolute Deviation," *Journal of the American Statistical Association*, vol. 88, no. 424, pp. 1273–1283, 1993. Publisher: [American Statistical Association, Taylor & Francis, Ltd.].